Integrated and computationally-efficient analysis method for FRP building floor panels

Ali Sadrara[a,*], Hamed Khezrzadeh[b], and Massood Mofid[a]

a. *Center of Excellence in Structures and Earthquake Engineering, Department of Civil Engineering, Sharif University of Technology, Tehran, Iran.*
b. *Faculty of Civil and Environmental Engineering, Tarbiat Modares University, Tehran, Iran.*

Abstract. Due to the many advantages of Fiber Reinforced Polymer (FRP) decks, such as lightweight and high strength, recently, using FRP decks as building deck panels is considered an alternative choice to traditional decks. Accordingly, there is an increasing need for an analysis tool for engineering and academic applications. Finite element is an accurate and reliable method for analyzing FRP decks. However, high computational cost and modeling difficulty somewhat limit its application. To overcome this shortcoming, this study presents an integrated, easy-to-use, computationally-efficient, and yet rather accurate analysis method for FRP decks. This integrated method was implemented in a computer code and can be easily used to analyze building FRP deck panels. To evaluate the deck's applicability as a building floor panel system, some requirements are needed to be met, including maximum allowable elastic deflection, local stability of components, vibration frequency, and ductility of the flooring system. The proposed method uses the Rayleigh-Ritz method to calculate these requirements. Using three different FRP deck examples, it was shown that the proposed method is generic and capable of analyzing various forms of the FRP deck panels, including all-FRP and hybrid decks made of two or more different materials.

1. Introduction

Fiber Reinforced Polymers (FRPs) in form of composite structures have found many applications in the construction industry because of their special characteristics such as high specific strength and modulus, high corrosion resistance, and low thermal conductivity [1]. One of their applications is in panelized construction such as bridge decks made from FRPs [2]. Yang and Sebastian [3] measured the deflection of an all-FRP pultruded Glass Fiber Reinforced Polymer (GFRP) bridge deck under tire loading. Gopinath et al. [4] proposed all-FRP deck panels using hybrid glass and jute fibers and compared the deflection of several cross-sections. Xin et al. [5] optimized an all-FRP bridge deck on steel girders. The objective

*. Corresponding author. Tel.: +98 21 82884971
E-mail addresses: ali.sadrara@sharif.edu (A. Sadrara);
khezrzadeh@modares.ac.ir (H. Khezrzadeh);
Mofid@sharif.edu (M. Mofid)

of the optimization was to maximize the bridge span and minimize the construction cost. Sa et al. [6] assessed the transverse bending and in-plane shear an all-GFRP pultruded bridge deck panels. They showed that the deck exhibited reliable and consistent flexural and shear behavior. Wang et al. [7] proposed and optimized an all-GFRP bridge deck panel on GFRP girders and showed that the proposed bridge panel meets the requirements of the design codes. Sun et al. [8] studied the web local buckling of all-GFRP bridge deck panels as one of the major failure modes. They investigated the influential parameters on local web buckling and failure modes under concentrated load. Park et al. [9] studied the behavior of adhesive joints in all-GFRP bridge deck panels. They checked the behavior of the joints at the serviceability and ultimate limit states.

Recently using FRP decks in building flooring systems drew researchers' attention. Gao et al. [10] proposed a Carbon Fiber Reinforced Polymer (CFRP) deck for application in building structures. Awad et al. [11] proposed a GFRP sandwich panel which is made of modified phenolic core and E-CR glass skins for the flooring system. Satasivam et al. [12,13] investigated modular web-flange FRP-steel composite systems fabricated of adhesively bonded pultruded profile sandwiched between two flat panels. Using composite FRP decks in building flooring systems yields a lighter and more resilient structures [14].

Although the FRPs exhibit superior properties in comparison to ordinary structural materials, there are some weak points that their influence should be mitigated, including their low ductility and relatively lower stiffness in some directions. To overcome these deficiencies, the idea of using hybrid FRP composite materials in decks has been proposed [15]. In hybrid FRP composites, two (or more) different materials are used to improve the mechanical properties. Ji et al. [16] investigated the static and fatigue behavior of the hybrid steel-FRP bridge deck. They proposed a deck with upper and lower GFRP facings and hybrid core of GFRP grid and multiple steel box cells and it is revealed that this deck exhibit certain improvements in comparison to the common all-FRP bridge decks. Lombardi and Liu [17] studied the elastic properties of a GFRP bridge deck and tried to increase the stiffness of the deck by embedding steel in its cross-section. The effect of using steel tubes in the core and embedding steel plates in the facesheet was also investigated by Lombardi and Liu [17]. The results indicated that using the hybrid system has increased the shear and flexural stiffness of the deck. There is other research devoted to experimental and numerical investigation of the hybrid composite deck made of concrete, steel, and FRP [18,19]. Kim and Lee [20] proposed and tested a hybrid steel-GFRP deck panel under monotonic and fatigue loads. They embedded steel wires into pultruded GFRP profiles and showed that this technic improved the behavior of the deck. Zou et al. [21] studied the shear behavior of a hybrid concrete-FRP deck panel and proposed design equations to predict its shear capacity. Pournasiri et al. [22] proposed a hybrid concrete-GFRP bridge deck panel. They investigated the influence of the configuration of the cross-section and concrete strength on the load-carrying capacity of the deck behavior. These research works concluded that the proposed hybrid steel-concrete-FRP deck is light and reliable. As a result, it is an appropriate choice for modular construction.

Several analytical methods are proposed to investigate FRP decks' behavior [23]. Barbero et al. [24] introduced a method to analyze an FRP deck/stringer bridge system. Kim and Lee [25] proposed an analytical model to investigate the flexural response of an FRP deck. Aref et al. [26] proposed a procedure, which is based on transformed plate formulation and the Ritz method, to analyze a skew FRP bridge deck with a parallel grid core. Xin et al. [27] conducted experimental, analytical, and numerical research on the flexural behavior of GFRP pultruded composite profiles for designing bridge decks. Satasivam et al. [28] presented an analytical approach for evaluation of the flexural behavior of modular GFRP sandwich assembly for two-way slab applications in which they used a symmetrical grillage model to simplify the aforementioned two-way slab as four beam members.

A brief overview of this paper is presented as follows: In § 2 the proposed analysis method is explained. In § 3, three comprehensive examples, including a sandwich panel, an all-FRP deck, and a hybrid steel-FRP are analyzed to check the applicability of the proposed analysis framework. Finally, conclusions are given in § 4.

2. Analysis and design procedure

There are four major steps in the delineated framework for the analysis and design of hybrid decks. These steps are described in detail in the following subsections.

2.1. Equivalent orthotropic plate

In order to reach the properties of deck equivalent plate, based on Zhou [29] two steps are designed. In the first step, the core of the deck is modeled as a plate with the same thickness as core thickness. This plate is denoted as a core equivalent plate. In the second step, the core equivalent plate and two facesheets are considered to form a sandwich plate. Finally, the deck equivalent plate properties are obtained by setting a sandwich plate equal to a single orthotropic plate. The properties of the deck equivalent plate that have been calculated in the previous steps are used in computing

deck deformation. The plate stiffness parameters are defined as follows:

$$D_x = \frac{I_x E_x}{L}, \quad D_y = \frac{I_y E_y}{L}, \quad D_{xy} = \nu_{xy} D_y, \qquad (1)$$

in which L is the width of the deck. Parameters I_x, E_x, and D_x are the moment of inertia, modulus of elasticity, and stiffness of plate in the x direction, respectively. It should be noted that x, y, and z-axes are along the length, width, and thickness of the deck, respectively. Parameter D_y is the stiffness of the plate in the y direction and D_{xy} is the stiffness of the plate in the xy plane. Parameter ν_{xy} is the axial in-plane Poisson's ratio. By using the above properties, the equivalent modulus of elasticity in x and y directions, in the case of core equivalent plate, are given as:

$$E_x^e = \frac{12 D_x (1 - \nu_{xy}\nu_{yx})}{H_C^3}, \qquad (2)$$

$$E_y^e = \frac{12 D_y (1 - \nu_{xy}\nu_{yx})}{H_C^3}, \qquad (3)$$

in which H_C is the thickness of the core equivalent plate and ν_{yx} is the transverse in-plane Poisson's ratio and is defined as:

$$\nu_{yx} = \frac{D_y}{D_x} \nu_{xy}. \qquad (4)$$

In the second step, the sandwich plate, which is consisted of two facesheets and a core equivalent plate is modeled by an equivalent orthotropic plate. Deck equivalent plate properties are calculated in terms of facesheets and core equivalent plate properties as follows:

$$E_x = \alpha_C E_x^e + \alpha_T E_x^f + \alpha_B E_x^f, \qquad (5)$$

$$E_y = \alpha_C E_y^e + \alpha_T E_y^f + \alpha_B E_y^f, \qquad (6)$$

in which E_x^f and E_y^f are the moduli of elasticity of the facesheets in x and y directions, respectively. Parameters α_C, α_T, and α_B are defined as:

$$\alpha_C = \frac{H_C}{H}, \quad \alpha_T = \frac{H_T}{H}, \quad \alpha_B = \frac{H_B}{H}, \qquad (7)$$

in which H_T, H_B, and H denote the thickness of top facesheet, bottom facesheet, and deck equivalent plate, respectively. The shear moduli of deck equivalent plate in xy, xz, and yz plane are written as follows:

$$G_{xy} = \alpha_C G_{xy}^e + \alpha_T G_{xy}^f + \alpha_B G_{xy}^f, \qquad (8)$$

$$G_{xz} = \left(\frac{\alpha_C}{G_{xz}^e} + \frac{\alpha_T}{G_{xz}^f} + \frac{\alpha_B}{G_{xz}^f} \right)^{-1}, \qquad (9)$$

$$G_{yz} = \left(\frac{\alpha_C}{G_{yz}^e} + \frac{\alpha_T}{G_{yz}^f} + \frac{\alpha_B}{G_{yz}^f} \right)^{-1}, \qquad (10)$$

in which G_{xy}^f, G_{xz}^f, and G_{yz}^f are the shear moduli of facesheets in xy, xz, and yz plane, respectively. Parameters G_{xy}^e, G_{xz}^e, and G_{yz}^e are the shear moduli of core equivalent plate in xy, xz, and yz plane, respectively. The shear modulus of the core equivalent plate can be calculated as:

$$G_{xz}^e = \frac{\sum\limits_{j=1}^{n} G_{xz}^j A_j}{A_P}, \qquad (11)$$

in which A_j is the area of jth component, which contributes to the shear stiffness in xz plane, and n is the number of these components. Parameter A_P is the cross-sectional area of the core equivalent plate which is perpendicular to x axis. Similarly, G_{xy}^e and G_{yz}^e can be calculated. It should be noted that, in the case of calculation of G_{xy}^e and G_{yz}^e, A_P is the area of a section of the core equivalent plate that is perpendicular to z and y axes, respectively.

2.2. Elastic deformation analysis

Calculation of the elastic deformation of a deck panel subjected to service load is an important part of the design and analysis process. Therefore, in this section, the procedure of calculation of elastic deflection of the deck is presented. In this study, the frameworks of both the Classical Lamination Plate Theory (CLPT) and First-order Shear Deformation Theory (FSDT) are implemented to calculate elastic deformation of the deck [30]. The displacement field (u,v,w) in CLPT is written as:

$$\begin{cases} u(x,y,z) = u_0(x,y) - z\left[\frac{\partial w_0}{\partial x}\right], \\ v(x,y,z) = v_0(x,y) - z\left[\frac{\partial w_0}{\partial y}\right], \\ w(x,y,z) = w_0(x,y), \end{cases} \qquad (12)$$

in which $u_0(x,y)$ and $v_0(x,y)$ are midplane displacements in x and y directions, respectively. In the case of calculation of the transverse deflection of symmetric laminates, these terms can be neglected. Parameter w_0 is the transverse displacement of the midplane in z direction. According to FSDT, a transverse plane that is normal to the midplane will not remain normal after deformation. The governing differential equations of symmetric laminates form a set of five simultaneous coupled equations. The generalized displacement field is defined as [31]:

$$\begin{cases} u(x,y,z) = u_0(x,y) + z\psi_x, \\ v(x,y,z) = v_0(x,y) + z\psi_y, \\ w(x,y,z) = w_0(x,y), \end{cases} \qquad (13)$$

in which $\psi_x = \frac{\partial u(x,y,z)}{\partial z}$ and $\psi_y = \frac{\partial v(x,y,z)}{\partial z}$ are rotations of a transverse normal about y and x axes, respectively. The dimensions of the deck in x and y directions are a and b, respectively. The imposed boundary conditions on the equivalent plate are:

$$x = 0, a \Rightarrow \begin{cases} M_x \approx -D_{22}\frac{\partial^2 w}{\partial x^2}|_{x=0,a} = -k_\theta \frac{\partial w}{\partial x}|_{x=0,a}, \\ w = 0, \\ \psi_y = 0, \end{cases} \quad (14)$$

$$y = 0, b \Rightarrow \begin{cases} M_y = D_{12}\frac{\partial^2 w}{\partial x^2} + D_{22}\frac{\partial^2 w}{\partial y^2} \\ \qquad +2D_{26}\frac{\partial^2 w}{\partial x \partial y} = 0, \\ V_y = D_{22}\frac{\partial^3 w}{\partial y^3} + 4D_{26}\frac{\partial^3 w}{\partial x \partial y^2} \\ \qquad +(4D_{66} + D_{12})\frac{\partial^3 w}{\partial y \partial x^2} = 0. \end{cases} \quad (15)$$

2.2.1. Shape functions

The first step to apply the Rayleigh-Ritz method is the selection of appropriate shape functions that can satisfy essential boundary conditions. Proper shape functions are generated by using the Gram-Schmidt process which generates orthonormal polynomials. Kumar et al. [32] presented this procedure for various boundary conditions. Orthonormal polynomial $\phi_j(\xi, \eta)$ is generated on the domains $0 \le \xi \le 1$ and $0 \le \eta \le 1$. Vector $\aleph$ is defined as:

$$\aleph = \begin{bmatrix} 1 & \xi & \eta & \xi^2 & \xi\eta & \eta^2 & \xi^3 & \xi^2\eta & \xi\eta^2 & \eta^3 \end{bmatrix}. (16)$$

The jth element of the vector is shown as $\aleph_j$. The shape functions are generated based on the boundary conditions by defining function $\Re$ as follows:

$$\Re = \xi^l (1 - \xi)^m \eta^n (1 - \eta)^p. \quad (17)$$

The values of l, m, n, and p depend on boundary conditions on $\xi = 0, 1$ and $\eta = 0, 1$, respectively and they can be denoted as 0, 1 and 2 for free, simply supported and clamped boundary conditions, respectively. Function $\wp_j$ is defined as:

$$\wp_j = \Re \, \aleph_j, \quad j = 1, 2, 3, \ldots. \quad (18)$$

ϕ_j is the jth polynomial shape function and calculated as:

$$\phi_1 = \wp_1, \quad (19)$$

$$\phi_j = \wp_j - \sum_{i=1}^{j-1} \varrho_{ji}\phi_i, \quad (20)$$

in which:

$$\varrho_{ji} = \frac{\langle \wp_j, \phi_i \rangle}{\langle \phi_i, \phi_i \rangle},$$

$$i = 1, 2, 3, ..., (j-1), \qquad j = 2, 3, 4, ..., N, \quad (21)$$

where $\langle \Theta_i, \Xi_j \rangle$ is the inner product of Θ_i, Ξ_j and is defined as follows:

$$\langle \Theta_i, \Xi_j \rangle = \int_0^1 \int_0^1 \Theta_i(\xi, \eta)\Xi_j(\xi, \eta)d\xi d\eta, \quad (22)$$

and the norm of $\|\phi_j\|$ is written as:

$$\|\phi_j\| = \langle \phi_j, \phi_j \rangle^{\frac{1}{2}} = \left\{ \int_0^1 \int_0^1 \phi_j(\xi, \eta)\phi_j(\xi, \eta)d\xi d\eta \right\}^{\frac{1}{2}}. (23)$$

The final form of the orthonormal polynomial is written as:

$$\hat{\phi}_j = \frac{\phi_j}{\|\phi_j\|}. \quad (24)$$

The generated shape functions are given in Appendix A.

2.2.2. Energy terms

The strain energy of the equivalent plate consists of three terms. The first term is strain energy due to the stretching of the mid-plane surface of the equivalent plate and can be calculated from:

$$V_S = \frac{1}{2}\int \{\varepsilon\}^T [A]\{\varepsilon\}dA, \quad (25)$$

in which $\{\varepsilon\}$ has the following definition:

$$\{\varepsilon\} = \left\{ \frac{\partial u}{\partial x} \quad \frac{\partial v}{\partial y} \quad \frac{\partial u}{\partial y} + \frac{\partial v}{\partial x} \right\}^T. \quad (26)$$

The second term is strain energy due to bending-stretching coupling. The structure of the deck and its equivalent plate in many practical cases are symmetric. Therefore, strain energy due to bending-stretching coupling is negligible. The last term that contributes to strain energy is the strain energy due to bending. The bending strain energy is expressed as:

$$V_B = \frac{1}{2}\int \{\hat{\kappa}\}^T [D]\{\hat{\kappa}\}dA, \quad (27)$$

in which $\{\hat{\kappa}\}$ is the curvature and is defined as follows:

$$\{\hat{\kappa}\} = \left\{ -\frac{\partial^2 w}{\partial x^2} \quad -\frac{\partial^2 w}{\partial y^2} \quad -\frac{\partial^2 w}{\partial x \partial y} \right\}^T. \quad (28)$$

In order to formulate the strain energy in non-dimensional form, the following non-dimensional parameters are defined [33].

$$\alpha = \frac{a}{b}, \ \beta = \frac{a}{H}, \ D_0 = \frac{E_0 H^3}{12(1 - \nu_{12}\nu_{21})},$$

$$d_{ij} = \frac{D_{ij}}{D_0}, \ \xi = \frac{x}{a}, \ \eta = \frac{y}{b},$$

$$\widehat{k_\theta} = \frac{ak_\theta}{D_0}, a_{ij} = \frac{a^2}{D_0}A_{ij}, \quad (29)$$

in which a and b are the dimensions in x and y directions of the rectangular plate and α is the plate aspect ratio. Parameters $D_{ij} - s$ and $A_{ij} - s$ are the elements of the D and A matrices, respectively. Parameter k_θ is the stiffness of the rotational springs

that are located along the edges of the deck equivalent plate. The non-dimensional form of the deflection is $\hat{w} = \frac{w}{H}$. In order to implement the Rayleigh-Ritz method, rotations and displacement are defined in the following series representation:

$$
\begin{cases}
\hat{w}(\xi, \eta) = \sum_{j=1}^{N} \phi_j(\xi, \eta)C_j, \\
\psi_\xi(\xi, \eta) = \sum_{j=1}^{N} \varsigma_j(\xi, \eta)M_j, \\
\psi_\eta(\xi, \eta) = \sum_{j=1}^{N} \iota_j(\xi, \eta)L_j,
\end{cases}
\tag{30}
$$

in which ϕ_j, ς_j, and ι_j are orthonormal polynomials that satisfy all prescribed essential boundary conditions and C_j, M_j, and L_j are unknown coefficients that can be calculated through the Rayleigh-Ritz method. Parameters ψ_ξ and ψ_η are the rotation of transverse normal about η and ξ axes, respectively. The uniformly distributed load is non-dimensionalized as $\hat{q}_0 = (a^4 q_0)/(D_0 H)$. The non-dimensional form of strain energy due to bending based on CLPT assumptions is obtained as:

$$
\begin{aligned}
\hat{V}_B = &\frac{1}{2} \int_0^1 \int_0^1 d_{11} \left(\frac{\partial^2 \hat{w}}{\partial \xi^2} \right)^2 + d_{22}\alpha^4 \left(\frac{\partial^2 \hat{w}}{\partial \eta^2} \right)^2 \\
&+ 4d_{66}\alpha^2 \left(\frac{\partial^2 \hat{w}}{\partial \eta \partial \xi} \right)^2 + 2d_{12}\alpha^2 \left(\frac{\partial^2 \hat{w}}{\partial \xi^2} \right) \left(\frac{\partial^2 \hat{w}}{\partial \eta^2} \right) \\
&+ 4d_{16}\alpha \left(\frac{\partial^2 \hat{w}}{\partial \xi^2} \right) \left(\frac{\partial^2 \hat{w}}{\partial \eta \partial \xi} \right) \\
&+ 4d_{26}\alpha^3 \left(\frac{\partial^2 \hat{w}}{\partial \eta^2} \right) \left(\frac{\partial^2 \hat{w}}{\partial \eta \partial \xi} \right) d\xi d\eta.
\end{aligned}
\tag{31}
$$

The bending energy based on FSDT assumptions is non-dimensionalized as follows

$$
\begin{aligned}
\hat{V}_B = &\frac{1}{2} \int_0^1 \int_0^1 \beta^2 d_{11}(\frac{\partial \psi_\xi}{\partial \xi})^2 + d_{22}(\alpha\beta)^2 \\
&(\frac{\partial \psi_\eta}{\partial \eta})^2 + 2d_{16}\beta^2 \frac{\partial \psi_\xi}{\partial \xi}(\frac{\partial \psi_\eta}{\partial \xi} + \alpha \frac{\partial \psi_\xi}{\partial \eta}) \\
&+ 2d_{26}\alpha\beta^2 \frac{\partial \psi_\eta}{\partial \eta}(\frac{\partial \psi_\eta}{\partial \xi} + \alpha\frac{\partial \psi_\xi}{\partial \eta}) + d_{66}\beta^2 \\
&(\alpha^2(\frac{\partial \psi_\xi}{\partial \eta})^2 + (\frac{\partial \psi_\eta}{\partial \xi})^2 + 2\alpha(\frac{\partial \psi_\xi}{\partial \eta})(\frac{\partial \psi_\eta}{\partial \xi})) \\
&+ a_{44}(\alpha^2(\frac{\partial \hat{w}}{\partial \eta})^2 + \beta^2 \psi_\eta^2 + 2\alpha\beta\psi_\eta \frac{\partial \hat{w}}{\partial \eta}) \\
&+ 2a_{45}(\alpha \frac{\partial \hat{w}}{\partial \eta} + \beta\psi\eta)(\frac{\partial \hat{w}}{\partial \xi} + \beta\psi_\xi) \\
&+ a_{55}\beta((\frac{\partial \hat{w}}{\partial \xi})^2 + \beta\psi_\xi^2 + 2\frac{\partial \hat{w}}{\partial \xi}\psi_\xi)d\xi d\eta.
\end{aligned}
\tag{32}
$$

The work done by external loads (i.e., uniformly distributed load on the applied zone (A_{q_0}) on the deck) is defined by:

$$
\hat{V}_q = \int_{A_{q_0}} \hat{q}_0 \hat{w}(\xi, \eta)d\xi d\eta.
\tag{33}
$$

The stored strain energy in the non-dimensional form is expressed as:

$$
\begin{aligned}
\hat{V}_\Gamma = &\frac{1}{2} \int_0^1 \beta\hat{k}_\theta \left[\frac{\partial \hat{w}}{\partial \xi}\bigg|_{\xi=0} \right]^2 d\eta \\
&+ \frac{1}{2} \int_0^1 \beta\hat{k}_\theta \left[\frac{\partial \hat{w}}{\partial \xi}\bigg|_{\xi=1} \right]^2 d\eta.
\end{aligned}
\tag{34}
$$

The total energy of the system subjected to uniformly distributed load in non-dimensional form is then written as:

$$
\hat{\Pi}_1 = \hat{V}_B - \hat{V}_q + \hat{V}_\Gamma + \hat{V}_S,
\tag{35}
$$

in which $\hat{V}_S$ is the non-dimensional form of V_S. In the deck systems, due to the nature of loading and boundary conditions, the deflection due to the stretch of the midplane is negligible. Consequently, its contribution is not significant and can be excluded without affecting the solution. To reach the complete displacement field solutions the total energy of the system is minimized with respect to $C_j - s$, $M_j - s$ and $L_j - s$. These unknown coefficients can be calculated by solving the following set of $3N$ simultaneous equation:

$$
\begin{cases}
\frac{\partial \hat{\Pi}_1}{\partial C_j} = 0, \\
\frac{\partial \hat{\Pi}_1}{\partial M_j} = 0, \\
\frac{\partial \hat{\Pi}_1}{\partial L_j} = 0.
\end{cases}
\tag{36}
$$

2.3. Stability analysis

As stated before, one of the most important requirements of floor decks is their components' stability. The stability of the components can also be evaluated by the Rayleigh-Ritz method. Some deck components are more prone to local buckling, and their stability should be checked. In many decks, among all of the components, facesheets are more vulnerable to local buckling. Therefore, in this section facesheet stability is considered. It is worth noting that the following calculation is not limited to the facesheets, and the stability of any slender component in compression can be checked according to the following procedure.

The bending-induced high compressive stresses in the center of the deck panel result in the possibility of local buckling events in the upper facesheet. The potential energy due to applied in-plane force is written as:

$$\hat{V}_L = \frac{1}{2} \int_0^1 \int_0^1 \lambda_x \left[\frac{\partial^2 \hat{w}(\xi, \eta)}{\partial \xi^2}\right]^2 d\xi d\eta, \qquad (37)$$

in which λ_x is the non-dimensional form of N_x and is defined as:

$$\lambda_x = -\left(\frac{a^2}{D_0}\right) N_x. \qquad (38)$$

In Figure 1 the critical buckling zone in the upper facesheet is shown. The boundary conditions of the upper facesheet in the critical zone are considered as simply supported and clamped along y axis and x axis, respectively [34].

The eigenfunctions of a beam with the same boundary conditions are assumed as primary shape functions. In most cases, it is reasonable to assume that boundary conditions of the upper facesheet along the length of the deck are clamped-clamped and along the width of the deck is simply supported. Accordingly, the eigenfunctions of a hinged-hinged beam and clamped-clamped beam are chosen as shape functions of the plate in x and y directions, respectively. The shape functions of the plate are presented in Appendix A. In this case, the total energy of the system will read as:

$$\hat{\Pi}_2 = \hat{V}_B + \hat{V}_L, \qquad (39)$$

in which $\hat{V}_B$ can be calculated based on the assumption of CLPT [35] or FSDT [17]. By minimizing the total energy of the system and solving the eigenvalue problem, the critical buckling load can be obtained.

2.4. Vibration analysis

Vibration analysis of the deck systems in both bridges and buildings is of great importance. One of the important design criteria in building floor panel systems is the vibration serviceability design. Floor vibration design is presented in AISC design guide 11 [36]. The first step of the vibration design is the calculation of the natural frequency of the deck system. In the modal analysis, the first mode is of the most importance. To calculate the first mode natural frequency of the deck, the total energy in the non-dimensional form is written as follows:

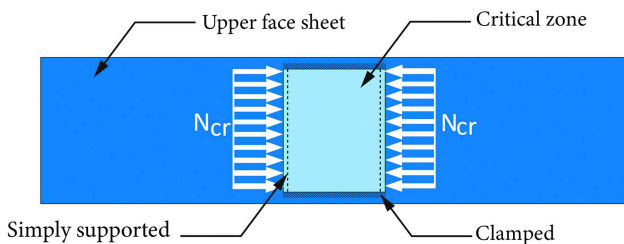$$\hat{\Pi}_3 = \hat{V}_B - \hat{V}_T + \hat{V}_\Gamma, \qquad (40)$$

Figure 1. Critical buckling zone in the upper facesheet.

in which $\hat{V}_T$ is the kinematic energy of the freely vibrating deck in non-dimensional form and can be read as:

$$\hat{V}_T = \frac{1}{2} \int_0^1 \int_0^1 \hat{w}^2 \Upsilon^2 d\xi d\eta, \qquad (41)$$

in which Υ is defined as:

$$\Upsilon = \frac{\omega a^2}{h} \sqrt{\frac{12\rho(1 - \nu_{12}\nu_{21})}{E_0}}, \qquad (42)$$

ω and ρ are the natural frequency and the equivalent mass density of the deck, respectively. In the calculation of natural frequency, orthonormal Gram-Schmidt polynomials are used as shape functions. After obtaining the natural frequency of the deck, the natural frequency of the floor panel system can be calculated for the vibration design of the floor panel systems. The natural frequencies of the joists, beams, and girders can be calculated through the fundamental natural frequency equation of simply supported and uniformly loaded beam as follows:

$$f_j = \frac{\pi}{2} \left[\frac{g E_s I_t}{Q L_b^4}\right]^{1/2}, \qquad (43)$$

in which g is the acceleration of gravity. Parameters E_s and I_t are modulus of elasticity of steel and transformed moment of inertia of beam section, respectively. Parameter Q is uniformly distributed line load and L_b is the length of the beam. The parameter f_j is the fundamental natural frequency of the joists (Hz). The natural frequency of the floor system can be calculated from the Dunkerley equation as follows:

$$\frac{1}{f_n^2} = \frac{1}{f_j^2} + \frac{1}{f_d^2}, \qquad (44)$$

in which f_j and f_d are the natural frequencies of the joists and the deck, respectively.

2.5. Ductility analysis

In this section, a procedure is presented to ensure that the hybrid deck exhibits ductile behavior by adding steel components to the deck due to their inherent ductile behavior. Figure 2 shows the schematic moment-curvature curve of a ductile deck in which curvature is divided into three ranges. In range 1 ($\kappa < \kappa_1$) the behavior is linear. The slope of the moment-curvature curve (K_b) in this region can be defined based on the elastic flexural stiffness of all constituents as:

$$K_b = \sum (EI)_{comp} + \sum (EI)_{st}, \qquad (45)$$

in which $\sum (EI)_{comp}$ and $\sum (EI)_{st}$ are the flexural stiffness of the composite and steel parts, respectively. In range 2 ($\kappa_1 < \kappa < \kappa_2$), steel parts start yielding, but the composite parts are still linear. The slope of
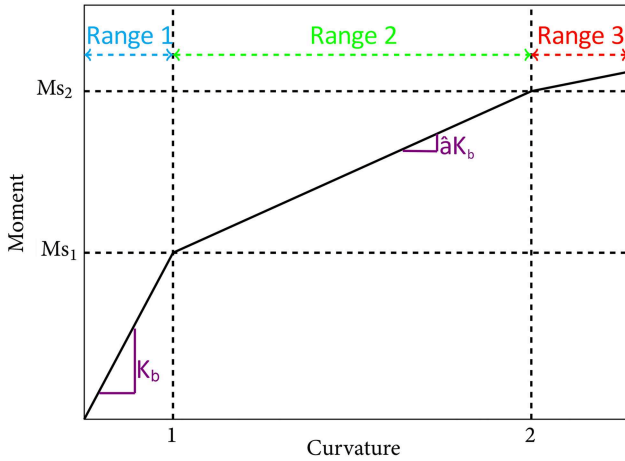
Figure 2. Schematic moment-curvature curve of a ductile hybrid deck.

the deck in this range is $\hat{a}K_b$. Term $\hat{a}$ is a degradation coefficient of the stiffness and will be calculated later. All of the steel parts yield a curvature of less than κ_2. At the beginning of the range 3 ($\kappa = \kappa_2$), composite parts start exhibiting nonlinear behavior.

In order to explicitly present the moment-curvature relationship, a parabolic function that passes through $(0, 0)$, (κ_1, M_{s1}), and (κ_2, M_{s2}) is written as follows:

$$\kappa = \Gamma_1^s M_s^2 + \Gamma_2^s M_s, \tag{46}$$

$$\Gamma_2^s = \frac{\kappa_1 - \kappa_2 \left[\frac{M_{s1}}{M_{s2}}\right]^2}{M_{s1} - M_{s2} \left[\frac{M_{s1}}{M_{s2}}\right]^2}, \tag{47}$$

$$\Gamma_1^s = \frac{\kappa_2 - M_{s2}\Gamma_2^s}{M_{s2}^2}. \tag{48}$$

The total moment that is the sum of the moment of steel and composite parts, reads as:

$$M_{total} = M_{st} + M_{comp}, \tag{49}$$

in which M_{total}, M_{st}, and M_{comp} are the total moment of the deck and the moment carried by steel parts and composite parts, respectively. In range 2, the total moment of the deck can be calculated as:

$$M_{total} = M_{st} + \kappa \sum (EI)_{comp}, \tag{50}$$

the differential of Eq. (50) with respect to the curvature results in:

$$\frac{\partial M_{total}}{\partial \kappa} = \frac{\partial M_{st}}{\partial \kappa} + \sum (EI)_{comp}. \tag{51}$$

As a result of steel yielding, the contribution of steel layers in flexural stiffness is almost negligible. Therefore, the term $\frac{\partial M_{st}}{\partial \kappa}$ can be neglected. Hence, the degradation factor is calculated as:

$$\hat{a} = \frac{\sum (EI)_{comp}}{\sum (EI)_{comp} + \sum (EI)_{st}}. \tag{52}$$

Degradation factor $\hat{a}$ is important in building flooring panel design to prevent sudden total failure of the system. Figure 3 shows a schematic view of an arbitrary section of a deck in which each layer can be steel or FRP laminate. The modulus of elasticity, width, thickness, and area of ith layer are denoted by E_i^L, b_i^L, t_i^L, and A_i^L, respectively. It should be noted that E_i^L of a composite laminate is the effective in-plane longitudinal modulus [37]. The location of the neutral axis in the elastic state (range 1) is calculated as:

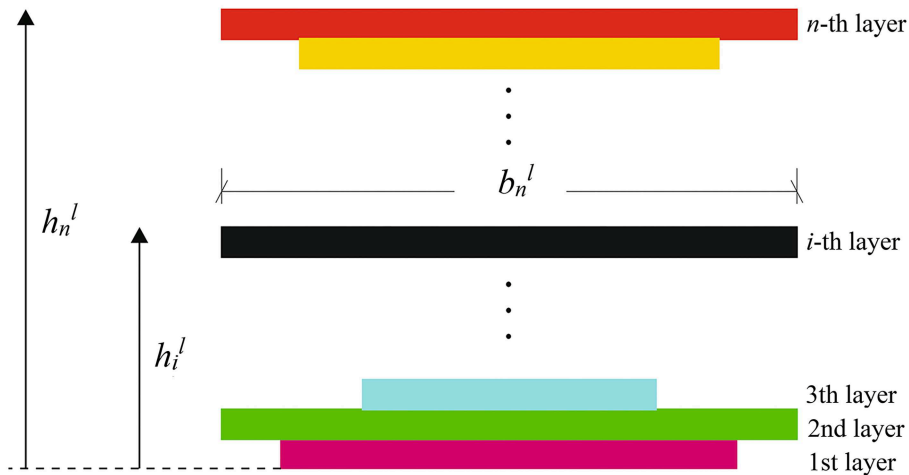$$\bar{h}_e = \frac{\sum_{i=1}^{n} A_i^L E_i^L \frac{h_i^L + h_{i-1}^L}{2}}{\sum_{i=1}^{n} A_i^L E_i^L}. \tag{53}$$

Figure 3. Schematic view of an arbitrary section of a deck.

In range 2, the location of the neutral axis is written as:

$$\bar{h}_p = \frac{\sum \left(A_k^L \sigma_k^L \frac{h_k^L + h_{k-1}^L}{2}\right)_{comp} + \sum \left(A_m^L \sigma_y^L \frac{h_m^L + h_{m-1}^L}{2}\right)_{st}}{\sum \left(A_k^L \sigma_k^L\right)_{comp} + \sum \left(A_m^L \sigma_y^L\right)_{st}}, \quad (54)$$

in which σ_y^L is the yield stress of the steel. Parameter κ_1 shown in Figure 2 is the minimum curvature in which the critical steel layer yields. Hence the yield curvature of all steel layers is calculated and its minimum value considered as κ_1.

$$\kappa_1 = \left[\frac{\varepsilon_y^{st}}{|h_{st-cr}^L - \bar{h}_e|}\right]_{\min}, \quad (55)$$

in which ε_y^{st} and h_{st-cr}^L are the yield strain and the position of the critical steel layer, respectively. Similarly, κ_2 shown in Figure 2 is the minimum curvature in which the critical composite layer fails which corresponds to the starting of the degradation process. Hence the failure curvature of all composite layers is calculated and its minimum value considered as κ_2.

$$\kappa_2 = \min \begin{cases} h_{comp-cr}^L - \bar{h}_p \geqslant 0 \Rightarrow \left[\frac{\varepsilon_{FPF-T}^{comp}}{h_{comp-cr}^L - \bar{h}_p}\right], \\ h_{comp-cr}^L - \bar{h}_p < 0 \Rightarrow \left[\frac{\varepsilon_{FPF-C}^{comp}}{\bar{h}_p - h_{comp-cr}^L}\right], \end{cases} (56)$$

in which $h_{comp-cr}^L$ is the position of the critical composite layer. Parameters $\varepsilon_{FPF-T}^{comp}$ and $\varepsilon_{FPF-C}^{comp}$ are the First Ply Failure (FPF) of the composite layer (laminate) in tension and compression, respectively. In this study, the Tsai-Wu failure criterion is used for FPF analysis of laminas of a composite layer (laminate). This criterion is written as [38]:

$$H_1 \sigma_1 SR + H_2 \sigma_2 SR + H_6 \tau_{12} SR + H_{11}(\sigma_1 SR)^2$$

$$+ H_{22}(\sigma_2 SR)^2 + H_{66}(\tau_{12} SR)^2$$

$$+ 2H_{12}(\sigma_1)(\sigma_2)SR^2 = 1, \quad (57)$$

in which H_1, H_2, H_6, H_{11}, H_{22}, H_{66}, and H_{12} are parameters that depend on the ultimate stresses of the laminae. The exact definition of these parameters and the procedure of FPF analysis are presented in [37] which is omitted here for the sake of brevity. The stress ratio is shown by SR.

It is assumed that all steel layers yielded before the whole section reaches a curvature of κ_2. This assumption can be checked by:

$$\left[\frac{\varepsilon_y^{st}}{|h_{st-last}^L - \bar{h}_e|}\right]_{\max} < \kappa_2, \quad (58)$$

$h_{st-last}$ is the position of the last steel layer to yield. The ductility factor of the deck is defined as:

$$\bar{\mu}_{deck} = \frac{\kappa_2}{\kappa_1}. \quad (59)$$

Based on the proposed method the ductility ($\bar{\mu}_{deck}$)

and degradation factor ($\hat{a}$) can be calculated. One of the limit states in the deck design is evaluating the nonlinear deflection of the deck subjected to high concentrated force. To calculate the deflection in the concentrated loading in linear and nonlinear range a procedure based on the nonlinear moment-area theorem is proposed in which the deck is considered as a simply supported beam.

$$\Delta_{NL} = \frac{X_L}{L_d} \int_0^{L_d} \kappa(x)(L_d - x)dx$$

$$- \int_0^{X_L} \kappa(x)(X_L - x)dx, \quad (60)$$

in which Δ_{NL} and L_d are deflection and length of the deck, respectively. The X_L is the distance between support and concentrated force. The curvature distribution is denoted by $\kappa(x)$, which can be calculated as follows:

$$\kappa(x) = \begin{cases} 0 \leq x \leq X_L \Rightarrow & \Gamma_1^s[P_{con}(1 - \frac{X_L}{L_d}x)]^2 \\ & + \Gamma_2^s[P_{con}(1 - \frac{X_L}{L_d}x)], \\ X_L \leq x \leq L_d \Rightarrow & \Gamma_1^s[P_{con}X_L(1 - \frac{x}{L_d})]^2 \\ & + \Gamma_2^s[P_{con}X_L(1 - \frac{x}{L_d})], \end{cases} (61)$$

in which P_{con} is the applied concentrated force. For different moment distributions, this function is changed accordingly. Since the input of this method is the moment distribution of the deck and moment-curvature of the cross-section, this procedure can be applied to reach the nonlinear load-deflection of arbitrary loading conditions. Substituting Eq. (61) in Eq. (60) results in:

$$\Delta_{NL} = \frac{P_{con}}{12} \left[\frac{X_L(X_L - L_d)}{L_d}\right]^2$$

$$[3X_L P_{con} \Gamma_1^s (L_d - X_L) + 4L_d \Gamma_2^s]. \quad (62)$$

To summarize the entire procedure, a flowchart is presented in Figure 4. This flowchart is used to develop the computer code to analyze FRP decks.

3. Applications

To implement the proposed method, three examples are presented. In the first example, a sandwich panel is analyzed. The second example is dedicated to the analysis of an all-FRP deck on supporting steel beams. In the third example, a hybrid steel-FRP deck with a complex geometry is analyzed from the material stage to the post-damage stage.

Finite element analysis is a well-known, reliable and widely-used method for analyzing different forms of structures [39–41]. Several examples can be found in the literature such as Patil et al. [42–44], Mysore et al. [45], Nimbagal et al. [46].
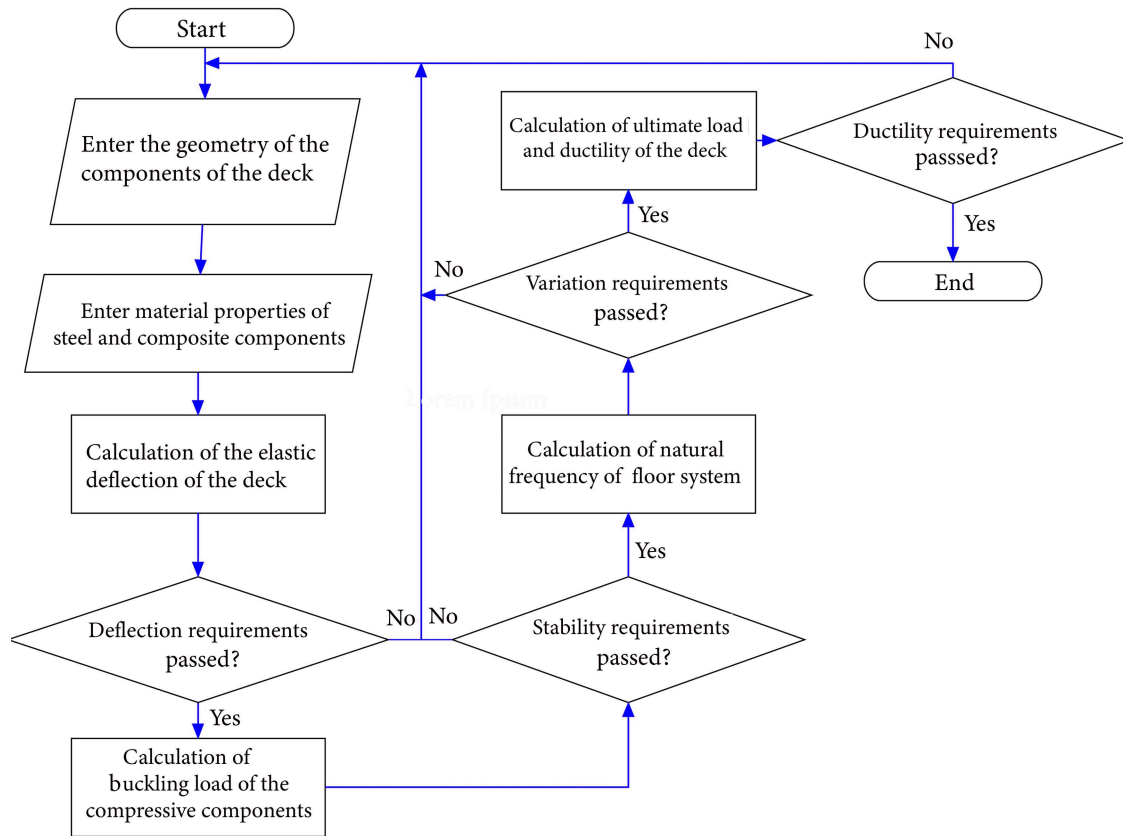
Figure 4. The flowchart of the proposed method.

High fidelity FEA is employed using Abaqus 6.14 software [47] to assess the accuracy of the proposed method in all examples. In the FEA, the deck's composite components are modeled using the 8-noded quadrilateral in-plane general-purpose continuum shell. The steel components are modeled using the 8-noded linear brick element of the 3D-stress family [48]. Through-thickness properties and layup of the composite components are modeled explicitly. The mesh sizes of 5 mm×5 mm and 10mm×10 mm are used to discretize composite and steel components, respectively. The contact behavior in components' interface is modeled using tie constraints.

3.1. Example 1

In this section, the applicability of the proposed framework is examined for sandwich panels. Several FRP sandwich panels for building floor systems are tested by Zhu et al. [49]. Specimen "*PAfb80-4-120*"

of the aforementioned study is considered here. This sandwich panel has GFRP facesheets and cores. The shear stiffness and strength of the core are increased by wooden blocks. The deck has simply supported edges on two opposite sides and has free boundary conditions in the other edges. The length and width of the specimen are 1.5 m and 0.48 m, respectively. The geometry of this sandwich panel is shown in Figure 5.

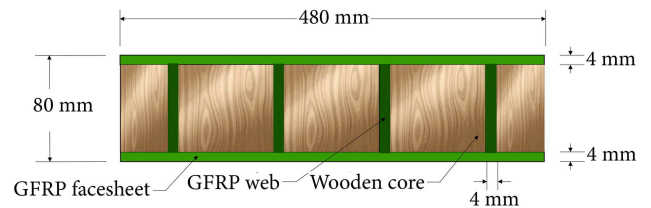The material properties of the sandwich panel components are presented in Table 1.

Figure 5. The geometry of the sandwich panel in Example 1 proposed by Zhu et al. [49].

Table 1. The material properties of the sandwich panel components tested by Zhu et al. [49]

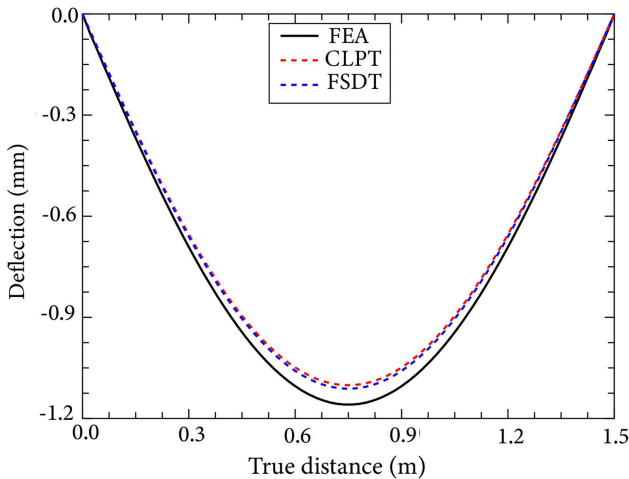| Material	E_1 (GPa)	E_2 (GPa)	E_3 (GPa)	ν_{12}	ν_{13}	ν_{23}	G_{12} (GPa)	G_{13} (GPa)	G_{23} (GPa)
GFRP facesheet	20.4	9.52	9.52	0.21	0.21	0.21	3.32	3.32	3.32
GFRP web	5.9	3.21	3.21	0.24	0.24	0.24	5.51	5.51	5.51
Wooden core	3.87	1.47	1.47	0.23	0.23	0.23	0.46	0.46	0.21

Figure 6. Deflection of deck versus deflection of the equivalent orthotropic plate in Example 1 subjected to uniformly distributed load.
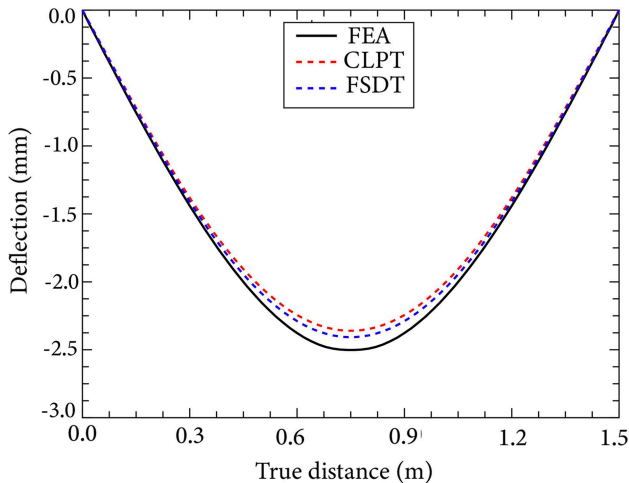

Figure 7. Deflection of deck vs. deflection of the equivalent orthotropic plate in Example 1 subjected to concentrated load.

3.1.1. Elastic deformation analysis
The elastic deflection of the deck subjected to uniformly distributed, 6 kN/m², and concentrated loads, 6.34 kN, are calculated based on CLPT and FSDT. The results are verified against FEA as shown in Figure 6 and Figure 7, respectively. Due to negligible shear deformations the results of CLPT and FSDT are approximately the same.

3.1.2. Vibration analysis
The first natural frequency of the sandwich panel including finishing and furniture is calculated as 161.89 rad/s using FEA. The natural frequency calculated by the Rayleigh-Ritz method is 169.15 rad/s which is in agreement with FEA results.

3.2. Example 2
To evaluate the applicability of the proposed method for all-FRP decks, in the second example, a floor panel system consists of an all-FRP deck and a supporting steel beam named "UA" in [13] is considered. In this case study, the proposed method is evaluated in the case of a pultruded composite deck. The geometry of this deck is shown in Figure 8. The deck has simply supported edges on two opposite sides and has free boundary conditions in other edges. The length and width of the specimen are 2.73 m and 0.5 m, respectively.

The deck is fabricated from pultruded GFRP materials. The axial modulus and transverse modulus of the facesheet are 31.7 GPa and 5.0 GPa, respectively. The axial modulus of the box profile is 32.2 GPa.

3.2.1. Elastic deformation analysis
The elastic deflection of the deck subjected to uniformly distributed (2.5 kN/m²) and concentrated load (1.36 kN) are calculated based on CLPT and FSDT and the results are verified against FEA as shown in Figures 9 and 10, respectively. As indicated in these plots, due to the high shear stiffness of the deck, the shear deformation is negligible and the results of CLPT and FSDT are approximately the same.

3.2.2. Stability analysis
In this section, the stability of the upper facesheet is considered that is a compressive component of the deck. Qiao and Shan [50] calculated the critical buckling load of a plate with clamped-clamped boundary conditions as:

$$N_{cr} = \frac{24}{b^2} \left[1.871\sqrt{D_{11}D_{22}} + (D_{12} + 2D_{66}) \right], \quad (63)$$

in which the critical aspect ratio of the clamped-clamped plate is written as:

$$\gamma_{cr} = 0.663 \left[\frac{m^4 D_{11}}{D_{22}} \right]^{\frac{1}{4}}, \quad (64)$$

in which m is the buckling mode number. The width of the critical part of the upper facesheet is 5 cm and based on Eq. (64) the critical length is calculated as 5.2 cm. The critical buckling load of the upper facesheet using the Rayleigh-Ritz method is calculated as $N_{cr} = 5160$ kN/m which is in agreement with that of Eq. (63) ($N_{cr} = 5149$ kN/m). The critical buckling load is higher than the failure load of the upper facesheet and the facesheet is buckling safe.

3.2.3. Vibration analysis
The first natural frequency of the deck, including finishing and furniture, is calculated as 63.38 rad/s using FEA. The natural frequency calculated by the Rayleigh-Ritz method is 66.42 rad/s, which is in agreement with the FEA simulations. The natural frequency of the supporting beam and floor panel system using Eq. (43) and Eq. (44) are 63.07 rad/s and 45.7 rad/s, respectively.
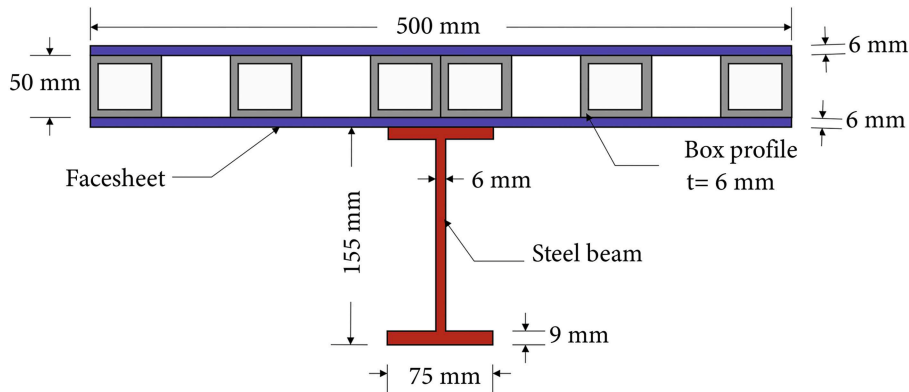
Figure 8. The geometry of the all-FRP deck in Example 2 proposed by Satasivam et al. [13].
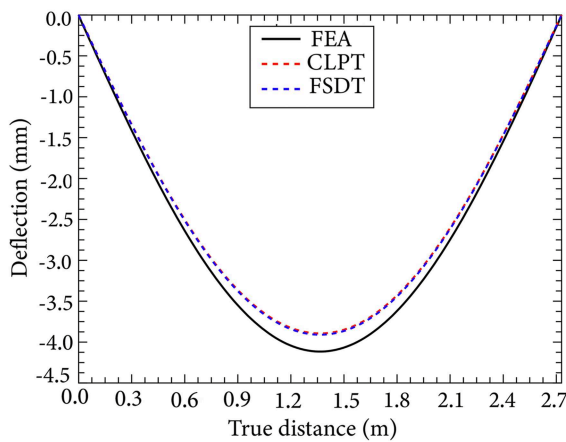

Figure 9. Deflection of deck vs. deflection of the equivalent orthotropic plate in Example 2 subjected to uniformly distributed load.
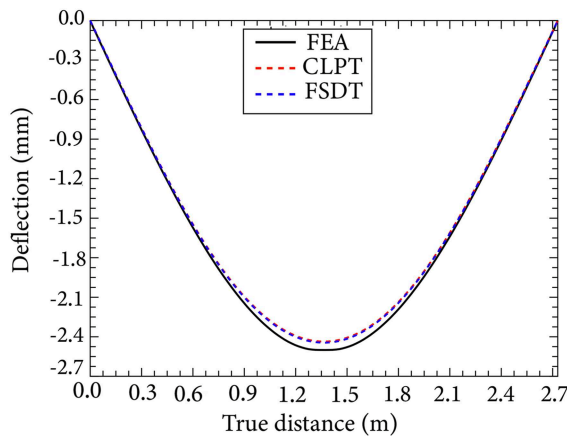

Figure 10. Deflection of deck vs. deflection of the equivalent orthotropic plate in Example 2 subjected to concentrated load.

3.3. Example 3

In this section, a hybrid deck with novel and complex geometry is analyzed and designed to indicate the applicability of the proposed method. The dimension and geometry of the deck are shown in Figure 11.

3.3.1. Material and stacking sequence

It is assumed that this deck is composed of composite materials and steel. GFRP material has the advantages of composite materials and has a lower cost, which is a very important parameter in building construction. Hence, using GFRP materials is more reasonable. Axial modulus, transverse modulus, axial Poisson's ratio, axial shear modulus, and the specific gravity of the GFRP are 37.55 GPa, 5.68 GPa, 0.25, 2.19 GPa, and 1.98, respectively. The orientations of the fibers of the facesheet laminates are selected of 60% $0°$, 20% $\pm45°$ and 20% $90°$. The orientations of the fibers of the core laminate are selected of 66% $\pm45°$ and 34% $0°$ [51]. The facesheets consist of 40 plies with the stacking of $[0_6/+45/-45/90_2]_{2s}$. The core laminate is comprised of 24 plies with the stacking of $[+45/-45/+45/-45/0_2]_{2s}$. Steel parts are considered to be made from A36 steel [52].

3.3.2. Elastic deformation analysis

The elastic deflection of the deck is calculated based on the proposed method, and FEA is used to check its accuracy. The deflections of the deck subjected to distributed and concentrated loads calculated by the Rayleigh-Ritz method and FEA are compared in Figures 12 and 13, respectively. It should be noted that the concentrated load is located at the center of the upper facesheet. It can be seen that the proposed method can calculate deflection accurately.

As shown in Figure 13, applying concentrated load results in high shear stress in the vicinity of the load causing extreme local deformations, but cannot be captured by the shape functions used in the study. The proposed analysis method aims to calculate the deformation accurately with low computational cost and was found to have acceptable accuracy for maximum deformation, so local effects of concentrated loads were neglected.

3.3.3. Stability analysis

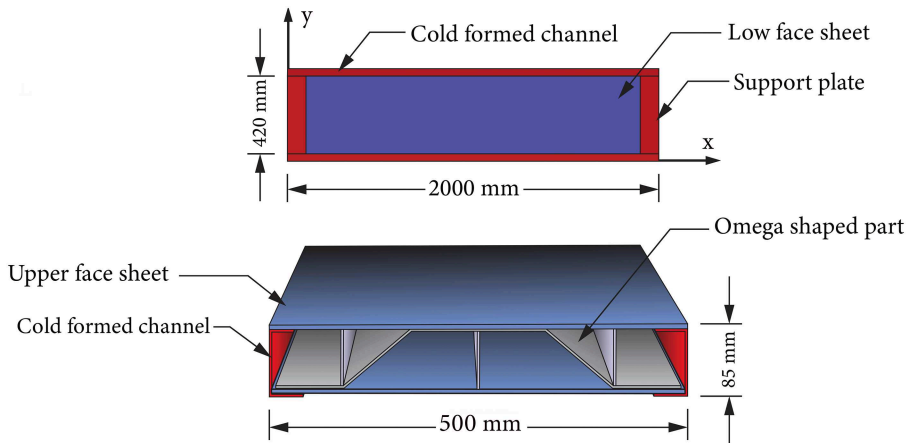The critical buckling load of the upper facesheet is

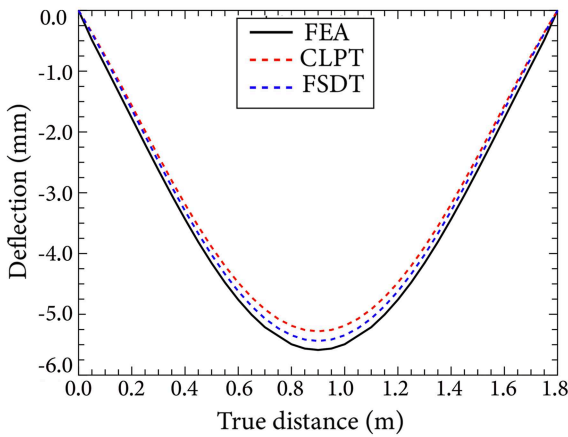**Figure 11.** The geometry of the deck in Example 3 (3D and bottom views).

Figure 12. Deflection of deck vs. deflection of the equivalent orthotropic plate in Example 3 subjected to uniformly distributed load.
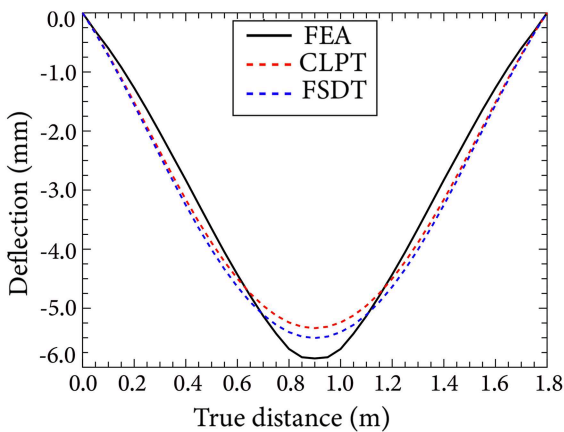

Figure 13. Deflection of deck vs. deflection of the equivalent orthotropic plate in Example 3 subjected to concentrated load.

calculated as: N_{cr}=63.53 kN/m. The critical buckling load calculated by Eq. (63) is N_{cr}=63.36 kN/m. Therefore, the value of critical buckling load obtained from the Rayleigh-Ritz method agrees with the result

obtained from Eq. (63). The critical buckling load is higher than the failure load of the upper facesheet.

3.3.4. Vibration analysis

The first natural frequency of the deck, including finishing and furniture as well as live load obtained through the Rayleigh-Ritz method, is 254.97 rad/s which shows good agreement with the results of finite element (251.35 rad/s).

3.3.5. Ductility analysis

The first step in ductility analysis is calculating the damage initiation and yield strains of composite and steel layers, respectively. Therefore, FPF analysis is implemented to calculate the post-damage behavior of laminates. The FPF shows that the stress-strain curve of the core laminates has a degradation in the stiffness in the strain of 0.006, which is dedicated to the failure of $\pm 45°$ laminas. The fracture strain of the laminae of the core is 0.018 in which 0° laminas fail. The stress-strain curve of the facesheet laminas shows two-point of degradation in strains of 0.004 and 0.007 which are corresponding to the failure of 90° laminas and $\pm 45°$ laminas, respectively. The fracture strain of the facesheet laminate is equal to 0.18 in which 0° laminas fail. It is worth noting that the yield strain of the steel is equal to 0.0012. The values of κ_1 and κ_2, using Eq. (55) and Eq. (56), are calculated as 0.031 and 0.098, respectively. The degradation and ductility factors using Eq. (52) and Eq. (59) of the deck are calculated as 0.61 and 3.13, respectively. The plastic analysis method which has been presented in Ref. [53] is used to calculate the moment-curvature relationship of steel layers. In this method, the steel sections are meshed by horizontal lines, which divide the flanges of steel channels into 4 strips and webs of the steel part into 16 strips. In ranges 1 and 2, the composite layers are elastic and their corresponding flexural stiffness is added to steel layers. Further information about
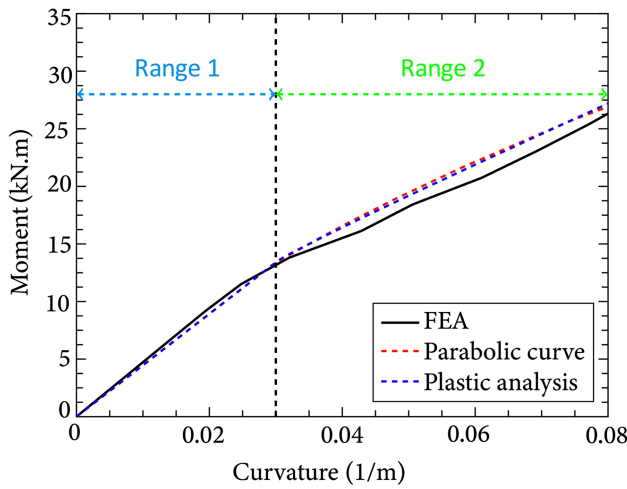
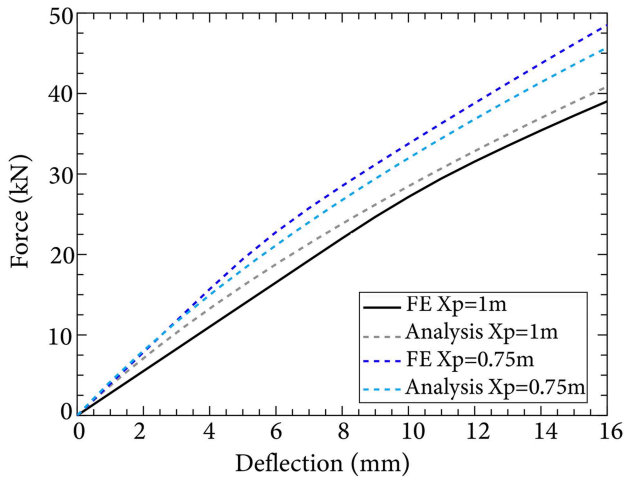**Figure 14.** Moment-curvature diagram of the deck section.

Figure 15. The load-deflection curve of the deck subjected to concentrated load.

this method can be found in Ref. [53]. The moment-curvature curve of the deck section acquired from FEA and the proposed method is compared in Figure 14. As it can be seen, the proposed analytical method can accurately calculate the nonlinear moment-curvature of the deck section.

The parabolic curve calculated by Eq. (46) is also shown in Figure 14. The values of Γ_1^s and Γ_2^s parameters are calculated as 5.24×10^{-5} kN^{-2}.m^{-3} and 1.54×10^{-3} kN^{-1}.m^{-2}, respectively. To calculate the nonlinear load-deflection curve of the deck, it is considered that the deck is subjected to a concentrated force that is located at arbitrary positions. The nonlinear load-deflection graphs of the deck, calculated by FEA and Eq. (62), with X_L=1 m and X_L=0.75 m are compared in Figure 15. The case of concentrated force located at the center of the upper facesheet is the critical loading case. As shown, the proposed method can predict the nonlinear deflection of the deck accurately.

4. Conclusions

This study presents an integrated analysis method for building Fiber Reinforced Polymer (FRP) deck panels. This method was implemented in a computer code and was used to analyze three different building FRP deck panels to evaluate their accuracy and versatility. These decks included a sandwich panel, a pultruded all-FRP deck, and a hybrid-steel FRP deck with laminar FRP. The results showed that the proposed integrated method is computationally-efficient and accurate. This method takes into account four requirements, including the elastic deflection, the stability of the components, the vibration characteristics, and the ductility of the deck. The main conclusions of this study are as follows:

- The elastic deflection was calculated using the Rayleigh-Ritz method with Gram-Schmidt shape functions. Results from Finite Element Analysis (FEA) and the proposed method were compared for three examples, showing similar maximum elastic deflections under uniform loading with a maximum difference of 0.04 mm;

- The stability of the deck components was calculated by the Rayleigh-Ritz method with beam eigenfunctions. The critical local buckling loads of the components of examples 2 and 3 calculated by the existing equations in the literature are 5149.0 kN/m and 63.5 kN/m. The proposed method calculated this parameter as 5160.0 kN/m and 63.4 kN/m, respectively;

- The natural frequency, which plays a pivotal role in the vibration characteristics of the decks, is calculated using the Rayleigh-Ritz method with Gram-Schmidt shape functions. According to FEA, the natural frequency in examples 1, 2, and 3 equal 161.89 rad/s, 63.38 rad/s, and 251.35 rad/s. The proposed method calculated the natural frequencies as 169.15 rad/s, 66.42 rad/s, and 254.97 rad/s;

- A novel method was proposed to ensure the ductile behavior of the deck and was used to calculate the nonlinear load deflection for one example. Results were compared to those from FEA.

The proposed method showed comparable results to FEA and had a lower computational cost. It can be used to analyze various FRP deck panels with high accuracy and ease of use, without requiring expertise in FE modeling.

References

1. Van Den Einde, L., Zhao, L., and Seible, F. "Use of FRP composites in civil structural applications", *Constr. Build. Mater.*, **17**(6), pp. 389–403 (2003). DOI: 10.1016/S0950-0618(03)00040-0.

2. Saleem, M.A., Zafar, M.N., Saleem, M.M., and Xia, J. "Recent developments in the prefabricated bridge deck systems", *Case Stud. Constr. Mater.*, **15**, p. e00750 (2021). DOI: 10.1016/j.cscm.2021.e00750.

3. Yang, Z. and Sebastian, W. "Nonlinear behaviour of pultruded decks due to morphing of tyre loads", *Eng. Struct.*, **274**, p. 115146 (2023). DOI: 10.1016/j.engstruct.2022.115146.

4. Gopinath, R., Poopathi, R., and Saravanakumar, S.S. "Characterization and structural performance of hybrid fiber-reinforced composite deck panels", *Adv. Compos. Hybrid Mater.*, **2**(1), pp. 115–124 (2019). DOI: 10.1007/s42114-019-00076-w.

5. Xin, H., Mosallam, A., Correia, J.A.F.O., et al. "Material-structure integrated design optimization of GFRP bridge deck on steel girder", *Structures*, **27**, pp. 1222–1230 (2020). DOI: 10.1016/j.istruc.2020.07.008.

6. Sa, M.F., Correia, J.R., Silvestre, N., et al. "Transverse bending and in-plane shear behaviours of multicellular pultruded GFRP deck panels with snap-fit connections", *Thin-Walled Struct.*, **154**, p. 106854 (2020). DOI: 10.1016/j.tws.2020.106854.

7. Wang, J., Cheng, B., Yan, X., et al. "Structural analysis and optimization of an advanced all-GFRP highway bridge", *Structures*, **34**, pp. 3155–3171 (2021). DOI: 10.1016/j.istruc.2021.09.064.

8. Sun, Y., Liu, Y., Wang, C., et al. "Web buckling mechanism of pultruded GFRP bridge deck profiles subjected to concentrated load", *Structures*, **34**, pp. 3789–3805 (2021). DOI: 10.1016/j.istruc.2021.10.002.

9. Park, S.-Z., Jeong, S.-H., Lee, H., et al. "Analysis of adhesive joints in a GFRP bridge deck under bidirectional bending due to traffic wheel loads", *Appl. Sci.*, **12**(5), p. 2748 (2022). DOI: 10.3390/app12052748.

10. Gao, Y., Chen, J., Zhang, Z., et al. "An advanced FRP floor panel system in buildings", *Compos. Struct.*, **96**, pp. 683–690 (2013). DOI: 10.1016/j.compstruct.2012.09.033.

11. Awad, Z.K., Aravinthan, T., and Zhuge, Y. "Experimental and numerical analysis of an innovative GFRP sandwich floor panel under point load", *Eng. Struct.*, **41**, pp. 126–135 (2012). DOI: 10.1016/j.engstruct.2012.03.023.

12. Satasivam, S., Bai, Y., and Zhao, X.-L. "Adhesively bonded modular GFRP web–flange sandwich for building floor construction", *Compos. Struct.*, **111**, pp. 381–392 (2014). DOI: 10.1016/j.compstruct.2014.01.003.

13. Satasivam, S. and Bai, Y. "Mechanical performance of modular FRP-steel composite beams for building construction", *Mater. Struct.*, **49**(10), pp. 4113–4129 (2016). DOI: 10.1617/s11527-015-0776-2.

14. Hollaway, L.C. "A review of the present and future utilisation of FRP composites in the civil infrastructure with reference to their important in-service properties", *Constr. Build. Mater.*, **24**(12), pp. 2419–2445 (2010). DOI: 10.1016/j.conbuildmat.2010.04.062.

15. Zou, X., Lin, H., Feng, P., et al. "A review on FRP-concrete hybrid sections for bridge applications", *Compos. Struct.*, **262**, p. 113336 (2021). DOI: 10.1016/j.compstruct.2020.113336.

16. Ji, H.S., Son, B.J., and Ma, Z. "Evaluation of composite sandwich bridge decks with hybrid FRP-steel core", *J. Bridg. Eng.*, **14**(1), pp. 36–44 (2009). DOI: 10.1061/(ASCE)1084-0702(2009)14:1(36).

17. Lombardi, N.J. and Liu, J. "Glass fiber-reinforced polymer/steel hybrid honeycomb sandwich concept for bridge deck applications", *Compos. Struct.*, **93**(4), pp. 1275–1283 (2011). DOI: 10.1016/j.compstruct.2010.10.007.

18. Alizadeh, E. and Dehestani, M. "Detailed numerical modeling and parametric analysis of a composite deck", *J. Sandw. Struct. Mater.*, **20**(6), pp. 2077–2098 (2018). DOI: 10.1177/1099636218762686.

19. Alizadeh, E., Dehestani, M., Navayi Neya, B., et al. "Efficient composite bridge deck consisting of GFRP, steel, and concrete", *J. Sandw. Struct. Mater*, **21**(1), pp. 154–174 (2017). DOI: 10.1177/1099636216688347.

20. Kim, H.-Y. and Lee, S.-Y. "Static and fatigue load performance of a pultruded GFRP deck panel reinforced with steel wires", *Compos. Struct.*, **207**, pp. 166–175 (2019). DOI: 10.1016/j.compstruct.2018.09.022.

21. Zou, X., Feng, P., Bao, Y., et al. "Experimental and analytical studies on shear behaviors of FRP-concrete composite sections", *Eng. Struct.*, **215**, p. 110649 (2020). DOI: 10.1016/j.engstruct.2020.110649.

22. Pournasiri, E., Pham, T.M., and Hao, H. "Behavior of Ultrahigh-Performance Concrete Bridge Decks with New Y-Shape FRP Stay-in-Place Formworks", *J. Compos. Constr.*, **26**(3), p. 4022023 (2022). DOI: 10.1061/(ASCE)CC.1943-5614.0001214.

23. Fascetti, A., Feo, L., and Abbaszadeh, H. "A critical review of numerical methods for the simulation of pultruded fiber-reinforced structural elements", *Compos. Struct.*, **273**, p. 114284 (2021). DOI: 10.1016/j.compstruct.2021.114284.

24. Barbero, E.J., Satasivam, S., Bai, Y., et al. "A systematic analysis and design approach for single-span FRP deck / stringer bridges", *Compos. Struct.*, **31**(4), pp. 736–746 (2016). DOI: 10.1016/S1359-8368(99)00044-X.

25. Kim, Y. and Lee, J. "An analytical model for the flexural response of a fiber reinforced plastic deck using higher-order shear deformable plate theory", *Compos. Struct.*, **85**(4), pp. 275–283 (2008). DOI: 10.1016/j.compstruct.2007.10.035.

26. Aref, A.J., Alampalli, S., and He, Y. "Ritz-based static analysis method for fiber reinforced plastic rib core skew bridge superstructure", *-J. Eng. Mech.*, **127**(5), pp. 450–458 (2001). DOI: 10.1061/(ASCE)0733-9399(2001)127:5(450).

27. Xin, H., Mosallam, A., Liu, Y., et al. "Analytical and experimental evaluation of flexural behavior of FRP

pultruded composite profiles for bridge deck structural design", *Constr. Build. Mater.*, **150**, pp. 123–149 (2017). DOI: 10.1016/j.conbuildmat.2017.05.212.

28. Satasivam, S., Bai, Y., Yang, Y., et al. "Mechanical performance of two-way modular FRP sandwich slabs", *Compos. Struct.*, **184**, pp. 904–916 (2018). DOI: 10.1016/j.compstruct.2017.10.026.

29. Zhou, A. "Stiffness and strength of fiber reinforced polymer composite bridge deck systems", PhD Thesis, Virginia Polytechnic Institute and State University, VA, US (2002).

30. Herakovich, C.T., Mechanics of Fibrous Composites, Wiley (1997).

31. Liew, K.M. "Solving the vibration of thick symmetric laminates by Reissner/Mindlin plate theory and thep-Ritz method", *J. Sound Vib.*, **198**(3), pp. 343–360 (1996). DOI: 10.1006/jsvi.1996.0574.

32. Kumar, A., Panda, S.K., and Kumar, R. "Buckling behaviour of laminated composite skew plates with various boundary conditions subjected to linearly varying in-plane edge loading", *Int. J. Mech. Sci.*, **100**, pp. 136–144 (2015). DOI: 10.1016/j.ijmecsci.2015.06.018.

33. Turvey, G.J. and Marshall, I.H., *Buckling and Post-buckling of Composite Plates*, Springer Science and Business Media (2012).

34. Garrido, M., Correia, J.R., Keller, T., et al. "Adhesively bonded connections between composite sandwich floor panels for building rehabilitation", *Compos. Struct.*, **134**, pp. 255–268 (2015). DOI: 10.1016/j.compstruct.2015.08.080.

35. Linghoff, D., Haghani, R., and Al-Emrani, M. "Carbon-fibre composites for strengthening steel structures", *Thin-walled Struct.*, **47**(10), pp. 1048–1058 (2009). DOI: 10.1016/j.tws.2008.10.019.

36. Murray, T.M., Allen, D.E., and Ungar, E.E., *Design guide 11: vibrations of steel-framed structural systems due to human activity*, 2nd Edn, pp. 7-14, American Institute of Steel Construction, US (2016).

37. Kaw, A.K., Mechanics of Composite Materials, 2nd Edn, pp. 369-431, CRC press, London, UK (2005).

38. Tsai, S.W. and Wu, E.M. "A general theory of strength for anisotropic materials", *J. Compos. Mater.*, **5**(1), pp. 58–80 (1971). DOI: 10.1177/002199837100500106.

39. Moghaddam, H., Sadrara, A., and Jalali, S.R. "Seismic performance of stainless-steel built-up box columns subjected to constant axial loads and cyclic lateral deformations", *Structures*, **33**, pp. 4080–4095 (2021). DOI: 10.1016/j.istruc.2021.07.014.

40. Moghaddam, H. and Sadrara, A. "Experimental and numerical evaluation of the mechanical characteristics of semi-rigid saddle connections", *Struct. Des. Tall Spec. Build.*, **31**(7), p. e1923 (2022). DOI: 10.1002/tal.1923.

41. Moghaddam, H. and Sadrara, A. "Improving the mechanical characteristics of semi-rigid saddle connections", *J. Constr. Steel Res.*, **186**, p. 106917 (2021). DOI: 10.1016/j.jcsr.2021.106917.

42. Patil, A.Y., Banapurmath, N.R., Sumukh, E.P., et al. "Multi-scale study on mechanical property and strength of new green sand (poly lactic acid) as replacement of fine aggregate in concrete mix", *Symmetry 2020.*, **12**(11), p. 1823 (2020). DOI: 10.3390/sym12111823.

43. Patil, V.S., Banoo, F., Kurahatti, R.V., et al. "A study of sound pressure level (SPL) inside the truck cabin for new acoustic materials: An experimental and FEA approach", *Alexandria Eng. J.*, **60**(6), pp. 5949–5976 (2021). DOI: 10.1016/j.aej.2021.03.074.

44. Patil, A.Y., Hegde, C., Savanur, G., et al. "Biomimicking nature-inspired design structures2014an experimental and simulation approach using additive manufacturing", *Biomimetics*, **7**(4), p. 186 (2022). DOI: 10.3390/biomimetics7040186.

45. Mysore, T.H.M., Patil, A.Y., Raju, G.U., et al. "Investigation of mechanical and physical properties of big sheep horn as an alternative biomaterial for structural applications", *Mater.*, **14**(14), p. 4039 (2021). DOI: 10.3390/ma14144039.

46. Nimbagal, V., Banapurmath, N.R., Sajjan, A.M., et al. "Studies on hybrid bio-nanocomposites for structural applications", *J. Mater. Eng. Perform.*, **30**(9), pp. 6461–6480 (2021). DOI: 10.1007/s11665-021-05843-9.

47. Documentation, A. and Manual, U. "Version 6.14", *Dassault Syst* (2010).

48. Barbero, E.J., *Finite Element Analysis of Composite Materials Using AbaqusTM*, CRC press (2013).

49. Zhu, D., Shi, H., Fang, H., et al. "Fiber reinforced composites sandwich panels with web reinforced wood core for building floor applications", *Compos. Part B Eng.*, **150**, pp. 196–211 (2018). DOI: 10.1016/j.compositesb.2018.05.048.

50. Qiao, P. and Shan, L. "Explicit local buckling analysis and design of fiber-reinforced plastic composite structural shapes", *Compos. Struct.*, **70**(4), pp. 468–483 (2005). DOI: 10.1016/j.compstruct.2004.09.005.

51. Keller, T. and Schollmayer, M. "Plate bending behavior of a pultruded GFRP bridge deck system", *Compos. Struct.*, **64**(3–4), pp. 285–295 (2004). DOI: 10.1016/j.compstruct.2003.08.011.

52. ASTM "Standard Specification for Carbon Structural Steel, ASTM A36/A36M-19", American Society for Testing and Materials, US (2019).

53. Wong, M.B. Plastic Analysis and Design of Steel Structures, Butterworth-Heinemann (2011).

54. Szilard, R., *Theories and Applications of Plate Analysis: Classical, Numerical and Engineering Methods*, John Wiley and Sons (2004).

Appendix A

Deflection shape functions [32]
The deflection shape functions are generated by using the Gram-Schmidt procedure. The following functions

are orthonormal and can fulfill the essential boundary conditions. The general behavior of these functions is based on the primary functions in which the essential boundary conditions are dedicated. The deflection shape functions are written as:

$$
\begin{cases}
\phi_1(\xi,\eta) = \iota_1(\xi,\eta) = 5.47(1-\xi)\xi, \\
\phi_2(\xi,\eta) = \iota_2(\xi,\eta) = \\
\quad \xi(-14.49 + 43.47\xi - 28.98\xi^2), \\
\phi_3(\xi,\eta) = \iota_3(\xi,\eta) = \\
\quad \xi(-9.48 + \eta(18.97 - 18.97\xi) + 9.48\xi), \\
\phi_4(\xi,\eta) = \iota_4(\xi,\eta) = \\
\quad \xi(28.46 - 161.27\xi + 265.63\xi^2 - 132.81\xi^3), \\
\phi_5(\xi,\eta) = \iota_5(\xi,\eta) = \\
\quad \xi(25.09 - 75.29\xi + 50.19\xi^2 \\
\quad +\eta(-50.19 + 150.59\xi - 100.39\xi^2)), \\
\phi_6(\xi,\eta) = \iota_6(\xi,\eta) = \\
\quad -12.24(1 - 6\eta + 6\eta^2)(-1+\xi)\xi, \\
\phi_7(\xi,\eta) = \iota_7(\xi,\eta) = \\
\quad \xi(-48.06 + 432.56\xi - 1249.62\xi^2 \\
\quad +1441.87\xi^3 - 576.75\xi^4), \\
\phi_8(\xi,\eta) = \iota_8(\xi,\eta) = \\
\quad \xi(-49.29 + 279.33\xi - 460.08\xi^2 + 230.04\xi^3 \\
\quad +\eta(98.59 - 558.67\xi + 920.17\xi^2 - 460.08\xi^3)), \\
\phi_9(\xi,\eta) = \iota_9(\xi,\eta) = \xi(-32.40 + 97.21\xi - 64.80\xi^2 \\
\quad +\eta^2(-194.42 + 583.26\xi - 388.84\xi^2) \\
\quad +\eta(194.42 - 583.26\xi + 388.84\xi^2)).
\end{cases} \tag{A.1}
$$

$$
\begin{cases}
\varsigma_1(\xi,\eta) = 1 \\
\varsigma_2(\xi,\eta) = -1.73 + 3.46\xi \\
\varsigma_3(\xi,\eta) = -1.73 + 3.46\eta \\
\varsigma_4(\xi,\eta) = -1.73 + 3.46\eta \\
\varsigma_5(\xi,\eta) = 2.23 - 13.41\xi + 13.41\xi^2 \\
\varsigma_6(\xi,\eta) = 3 - 6\xi + \eta(-6 + 12\xi) \\
\varsigma_7(\xi,\eta) = 2.23 - 13.41\eta + 13.41\eta^2 \\
\varsigma_8(\xi,\eta) = -3.87 + 23.23\xi \\
\quad -23.23\xi^2 + \eta(7.74 - 46.47\xi + 46.47\xi^2) \\
\varsigma_9(\xi,\eta) = -3.87 + \eta(23.23 - 46.47\xi) \\
\quad +7.74\xi + \eta^2(-23.23 + 46.47\xi)
\end{cases} \tag{A.2}
$$

Buckling shape functions [54]

The buckling shape functions are considered as beam eigenfunctions with the same boundary condition and are written as:

$$
\phi_{pq} = X_p Y_q, \quad p,q = 1,2,3,\dots, \tag{A.3}
$$

in which X_p and Y_q are the eigenfunctions of a hinged-hinged and a clamped-clamped beam, respectively.

The eigenfunctions of a hinged-hinged beam are calculated as follows:

$$
X_p = \sin(p\pi\xi), \tag{A.4}
$$

in which p is the number of modes and ξ is the non-dimensional form of the length of the beam. The eigenfunctions of a clamped-clamped beam are written as:

$$
Y_q = J(\lambda_q\eta) - \frac{J(\lambda_q)}{H(\lambda_q)}H(\lambda_q\eta), \tag{A.5}
$$

in which η is the non-dimensional form of the length of the beam. Parameters $H(\bullet)$ and $J(\bullet)$ are two functions and are defined as:

$$
\begin{cases}
H(\bullet) = \sinh(\bullet) - \sin(\bullet) \\
J(\bullet) = \cosh(\bullet) - \cos(\bullet)
\end{cases} \tag{A.6}
$$

Biographies

Ali Sadrara is a structural engineering researcher specializing in the seismic behavior of steel structures and advanced numerical modeling. He completed his MSc and PhD at Sharif University of Technology, where he investigated laminated FRP composite structures and conducted experimental and analytical studies on steel structural components. Currently, he focuses on machine learning applications in structural engineering and seismic design of steel systems. His work contributes to advancing sustainable and resilient infrastructure.

Hamed Khezrzadeh is an Assistant Professor of civil and structural engineering at Tarbiat Modares University. His current research interests include the application of innovative materials (SMAs, elastomers) in passive energy damping devices, micromechanical constitutive models of heterogeneous and periodic media, hybrid steel-FRP floor decks, structural health monitoring of FRP decks, and fracture mechanics.

Massood Mofid is a Renowned Professor of structural engineering at the Sharif University of Technology with expertise in the theory of plates and shells, structural dynamics, seismic behavior of structures, and numerical methods in structural engineering. He received his PhD in structural engineering from Rice University and has since made significant contributions to the field through his research and teaching. Professor Mofid has published numerous papers and articles in top-tier academic journals and is widely recognized in the area of structural engineering.